Monoallelic loss of tumor suppressor GRIM-19 promotes tumorigenesis in mice

Sudhakar Kalakonda[a,b,1], Shreeram C. Nallar[a,b,1], Sausan Jaber[c,d], Susan K. Keay[e,f], Ellen Rorke[a], Raghava Munivenkatappa[g,2], Daniel J. Lindner[h], Gary M. Fiskum[c], and Dhananjaya V. Kalvakolanu[a,b,3]

Departments of [a]Microbiology and Immunology, [c]Anesthesiology, [e]Medicine, and [g]Pathology, [b]Greenebaum Cancer Center, [d]Graduate Program in Biochemistry and Molecular Biology, University of Maryland School of Medicine, Baltimore, MD 21201; [f]Research Service, Veterans Administration Medical Center, Baltimore, MD 21201; and [h]Taussig Cancer Center, Cleveland Clinic Foundation, Cleveland, OH 44195

Edited by Robert D. Schreiber, Washington University School of Medicine, St. Louis, MO, and approved September 24, 2013 (received for review February 27, 2013)

Gene-associated with retinoid-interferon induced mortality-19 (GRIM-19), a STAT3-inhibitory protein, was isolated as a growth-suppressive gene product using a genome-wide expression knockdown screen. We and others have shown a loss of expression and occurrence of mutations in the *GRIM-19* gene in a variety of primary human cancers, indicating its potential role as tumor suppressor. To help investigate its role in tumor development in vivo, we generated a genetically modified mouse in which *Grim-19* can be conditionally inactivated. Deletion of *Grim-19* in the skin significantly increased the susceptibility of mice to chemical carcinogenesis, resulting in development of squamous cell carcinomas. These tumors had high Stat3 activity and an increased expression of Stat3-responsive genes. Loss of *Grim-19* also caused mitochondrial electron transport dysfunction resulting from failure to assemble electron transport chain complexes and altered the expression of several cellular genes involved in glycolysis. Surprisingly, the deletion of a single copy of the *Grim-19* gene was sufficient to promote carcinogenesis and formation of invasive squamous cell carcinomas. These observations highlight the critical role of GRIM-19 as a tumor suppressor.

cytokines | glucose metabolism | oxidative phosphorylation | immune response

It is now clear that multiple tumor suppressors are inactivated in a cell before the establishment of malignant state. The Hanahan–Weinberg model (1) suggests that at least 10 different genetic and microenvironmental alterations in and around a precancerous mammalian cell are necessary for successfully establishing a tumor. These alterations include the acquisition of resistance to apoptosis, enhanced motility, and angiogenesis; alteration in glucose metabolism; activation of tumor-proliferating inflammation; and suppression of antitumor immunity. Interestingly, a number of these processes are dependent on cytokines and/or other secretory factors, which alter tumor growth by changing the milieu around the tumor. Some cytokines inhibit and others promote tumor growth.

The IFN group of cytokines is a major player in suppressing neoplastic cell development (2). Endogenous IFNs act as sentinels against tumor development (3). IFNs not only induce growth-suppressive gene expression in the target tumor cells but also promote immune cell-mediated attack. Depending upon the target cell, IFNs can inhibit the progression of the cell cycle or can evoke apoptosis. IFN signaling defects are common in several human cancers (4). In certain cases IFN response is essential for tumor therapy with DNA-damaging agents (5); in other cases the expression of an IFN-related DNA-damage signature correlates with a lack of therapeutic response (6). Consistent with these activities, a number of IFN-regulated factors such as STAT1 (7) and the IFN-regulatory factors (IRF) IRF1 (8), IRF7 (9), and IRF8 (10) have been described as critical players in tumor suppression. The IRF1 and IRF8 proteins fit the classical definition of a tumor suppressor, given their loss of expression or mutation in primary human tumors and in animal models of cancer development (11, 12). All the proteins mentioned above are transcription factors whose activity/inactivity affects numerous gene products, and the products that are relevant to tumor suppression still need to be defined.

In several clinical and preclinical models, we and others have shown that IFN in combination with other modifiers of biological response, such as retinoic acid (RA), potently suppresses tumor growth (2). To investigate the mechanisms underlying tumor suppression, we used a genome-wide knockdown strategy and identified some potent growth suppressors. One such growth inhibitor was GRIM-19, a protein whose depletion and overexpression, respectively, promoted and suppressed tumor growth (13). GRIM-19 binds to STAT3 and inhibits its transcriptional activity (14, 15). Additionally, we and others have shown that GRIM-19 expression is lost in several primary tumors of lung, kidney, prostate, thyroid, ovary, colon, esophagus, and brain. More recently, we identified functionally inactivating somatic mutations of *GRIM-19* disrupting anti-STAT3 activity in certain human squamous oral cancers (16). To understand the importance of GRIM-19 in tumorigenesis, we developed a genetically modified mouse in which *Grim-19* can be conditionally inactivated. Using these mice, we show that loss of a single *Grim-19* allele is sufficient to promote skin tumorigenesis. These tumors exhibited mitochondrial respiratory dysfunction and altered energy metabolism. A number of genes associated with oncogenic glycolysis also were induced in these tumors in the absence of

Significance

Gene-associated with retinoid-interferon induced mortality-19 (GRIM-19) is an interferon-retinoid–regulated growth suppressor that inhibits cell growth by targeting the transcription factor STAT3 for inhibition. In primary human tumors *GRIM-19* is suppressed or mutated, leading to constitutive STAT3 activity and indicating the tumor-suppressive function of GRIM-19. To understand the in vivo role of Grim-19 in tumor development, we generated a *Grim-19* conditional knockout mouse. We found that deletion of even a single *Grim-19* allele is sufficient to augment skin tumorigenesis in mice, thus establishing a critical role for Grim-19 as a tumor suppressor. Tumors that developed in the absence of *Grim-19* exhibited mitochondrial respiratory chain dysfunction, elevated glycolysis, and Stat3-responsive gene expression.

Author contributions: S.K., S.C.N., G.M.F., and D.V.K. designed research; S.K., S.C.N., S.J., S.K.K., E.R., and D.J.L. performed research; S.K.K., E.R., D.J.L., and G.M.F. contributed new reagents/analytic tools; S.K., S.C.N., S.J., R.M., D.J.L., G.M.F., and D.V.K. analyzed data; and S.C.N. and D.V.K. wrote the paper.

The authors declare no conflict of interest.

This article is a PNAS Direct Submission.

[1]S.K. and S.C.N. contributed equally to this work.

[2]Present address: Division of Transplantation, Department of Surgery, The Johns Hopkins University School of Medicine, Baltimore, MD 21205.

[3]To whom correspondence should be addressed. E-mail: dkalvako@umaryland.edu.

This article contains supporting information online at www.pnas.org/lookup/suppl/doi:10.1073/pnas.1303760110/-/DCSupplemental.

Grim-19. This study shows the importance of a STAT3 inhibitor in preventing tumorigenesis.

Results

Generation of Mice with a Conditionally Inactivated *Grim-19* Allele. Because the direct deletion of *Grim-19* causes embryonic lethality, we designed a modified *Grim-19* allele that would allow the generation a tissue-specific knockout. The mouse *Grim-19* gene has five exons (E1–E5) and four introns. A significant portion of first two exons (E1 and E2) of *Grim-19* code for the 5′ UTR of the mature transcript, with the second exon (E2) coding for first 31 amino acids. Among the four introns, introns 2 and 3 are amenable to genetic manipulation. A targeting vector was designed to insert one loxP site in intron 2 (654 bp upstream of exon 3), and the other loxP site in intron 3 (203 bp downstream of exon 3), flanked by homologous arms of 1.7 kb and 3.2 kb, respectively. The neomycin-resistance gene (Neo) and the *Grim-19* gene E3 were flanked by the loxP sites. In presence of Cre recombinase, E3 and significant portions of introns 2 and 3 are deleted, and the remaining portion of the transcript goes out of frame, even though E4 and E5 are intact (Fig. 1 *A* and *B*).

This targeting construct was electroporated into C57BL6-derived ES cells, and positive clones were selected by Southern blot analysis (*SI Appendix*, Fig. S1). Correctly recombined stem cells were injected into the blastocysts of C57BL6 mice and transplanted into pseudopregnant mice. Several correctly targeted ES cell clones were injected into blastocysts to generate chimeras, which then were bred to obtain targeted ES cell-derived offspring carrying the modified *Grim-19* allele, as determined by PCR. Homozygous and heterozygous founder mice carrying the modified *Grim-19* allele ($Grim\text{-}19^{f}$) were used for further experimentation.

Generation of a Skin-Specific Knockout. To generate a skin-specific knockout, we mated $Grim\text{-}19^{f/f}$ mice with $K14\text{-}CreER^{tam}$ transgenic mice carrying the Cre recombinase fused to the ligand-binding domain of the estrogen receptor under the control of the *Keratin-14* (K14) promoter. Binding of the estrogen antagonist, 4-hydroxy tamoxifen (4-HT), activates the Cre recombinase, which then deletes the targeted region in the $Grim\text{-}19^{f/f}$ allele. We used a PCR-based approach to determine the genotype of the mice in all further experiments. To demonstrate the specificity of deletion, mice of the $Grim\text{-}19^{+/f}$ and *K14-Cre* genotypes were treated topically with 4-HT, and genomic DNA was collected from various tissues and subjected to PCR with allele-specific primers (*SI Appendix*, Table S1). In this experiment deletion generates heterozygous mice. PCR with wild-type ($^{+}$) and floxed (^{f}) allele-specific primers yielded the expected 353- and 200-bp products, respectively, in all tissues except skin, in which the 200-bp product was not observed. When the same DNA samples were used for PCR with a primer set that detects the deleted (KO) allele, the expected 253-bp product was observed in the skin but not in other tissues (*SI Appendix*, Fig. S1). The presence of *Cre* gene (235 bp) was ensured by PCR.

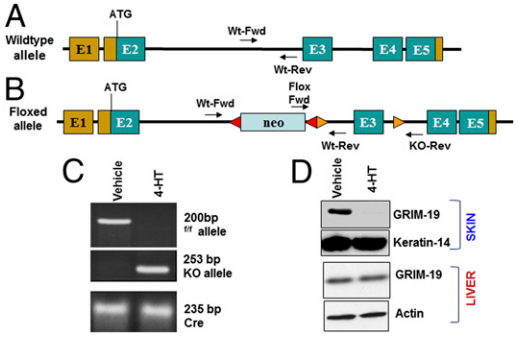

Fig. 1. Design and targeting of mouse *Grim-19*. (*A*) Organization of the *Grim-19* allele. The exonic regions of the gene are indicated as E1–E5. Greenish blue boxes show the protein-coding part of the gene; the mustard yellow boxes correspond to the UTR of the final transcript. (*B*) Modified *Grim-19* allele. Red and mustard yellow triangles indicate the Frt and LoxP target sites, respectively. Approximate locations of the specific primers that can distinguish wild-type, modified, and deleted alleles are indicated. (*C*) PCR analysis of the genomic DNA derived from mouse skins after treatment with vehicle (ethanol) or with 4-HT, which deletes the modified *Grim-19* locus. (*D*) Western blot analysis of the protein extracts from indicated tissues with specific antibodies. Keratin-14 and actin were used as internal controls for loading.

To determine if 4-HT caused the deletion of the *Grim-19* gene and its protein, $Grim\text{-}19^{f/f}$ mice with the *K14-Cre* gene were treated with ethanol (vehicle) or 4-HT, and genomic DNA from the skin samples was collected and used as a template for PCR with specific primers. As shown in Fig. 1*C*, 4-HT treatment specifically caused *Grim-19* gene deletion, as indicated by the disappearance of the $Grim\text{-}19^{f/f}$ allele and the appearance of the KO allele. These observations were confirmed further with a Western blot analysis of the skin- and liver-derived proteins. Consistent with the 4-HT–induced loss of the $Grim\text{-}19^{f/f}$ allele, the expression of Grim-19 protein was absent only in the skin and not in the liver (Fig. 1*D*). An equivalent expression of the K14 and actin proteins in the skin and liver, respectively, confirmed that the observed differences in GRIM-19 expression were not caused by uneven protein loading (Fig. 1*D*). Henceforth, the term "$Grim\text{-}19^{-/-}$ mice" connotes mice with the skin-specific deletion of *Grim-19*, i.e., $Grim\text{-}19^{f/f}$ *K14-Cre* mice treated with 4-HT.

Loss of *Grim-19* Did Not Significantly Affect Skin Differentiation. We next examined whether the deletion of *Grim-19* affects skin differentiation. Skins from control ($Grim\text{-}19^{f/f}$; notated as $Grim\text{-}19^{+/+}$) and 4-HT–treated ($Grim\text{-}19^{-/-}$) mice were sectioned and stained with the skin-specific markers keratin-1, K14, and filaggrin. These sections also were counterstained separately with H&E and DAPI to visualize tissue morphology and nuclei, respectively (Fig. 2 *A* and *B*). Except for some slightly increased cellularity in $Grim\text{-}19^{-/-}$ skins, formation of epidermis was normal in $Grim\text{-}19^{+/+}$ and $Grim\text{-}19^{-/-}$ mice (arrows in Fig. 2*A*). The expression of keratin-1 and filaggrin, which occur mainly in the epidermis, was comparable in both genotypes, as was K14, which is expressed in the epidermis and root follicles of the skin. In summary, Grim-19 is not required for skin differentiation or integrity.

Deletion of *Grim-19* Enhances Susceptibility to Skin Tumorigenesis. Because earlier clinical studies have shown that IFN/RA as a highly effective therapeutic on squamous cell carcinomas (SCCs) of skin and cervix (17, 18) and GRIM-19 is an IFN/RA-inducible gene product that is functionally inactivated in human SCCs of these organs (16, 19), we determined its role in the development of SCC. Functionally inactivating mutations in *GRIM-19* were found in oral SCCs in tobacco users. Because skin and the oral cavity are the first contact points with environmental carcinogens and because the dermal epithelium is continuous with head and neck and cervix, we used skin as a model for tumor studies. Furthermore, two of the carcinogens found in tobacco (20), benzanthracene and dibenzanthracene, are structural homologs of the tumor initiator 7,12-dimethylbenz[α]anthracene (DMBA). Thus, we reasoned that skin is an appropriate model for these studies. In the initial experiments groups of $Grim\text{-}19^{+/+}$ and $Grim\text{-}19^{-/-}$ mice ($n = 20$ per group) were observed for spontaneous development of skin tumors over a period of 19 mo. During that time, no tumors were found in these mice, irrespective of their genotype. Therefore, we next asked if these mice have any increased sensitivity to chemical carcinogens. Mice ($n = 24$ per group) were subjected to two-stage chemical carcinogenesis using a single topical dose of DMBA and twice-weekly doses of 12-O-tetradecanoylphorbol-13-acetate (TPA) for several weeks and were observed for tumor

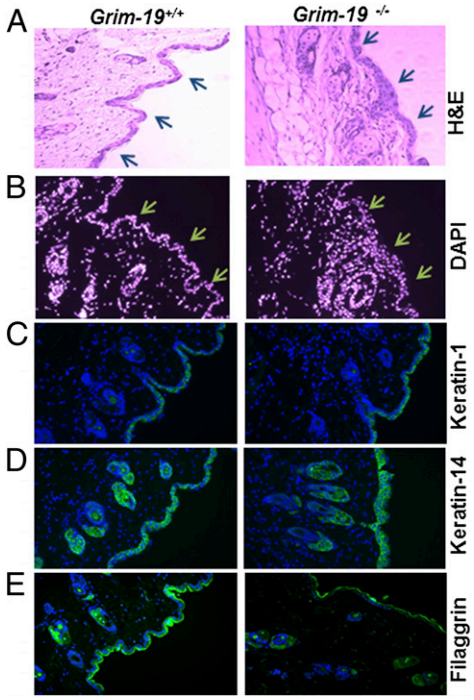

Fig. 2. Deletion of *Grim-19* does not affect skin organization. Skin sections from mice were stained with H&E (*A*), DAPI (*B*), or A7B- or Alexa Fluor (green fluorescence)-tagged secondary antibodies (*C–E*). In each case specific primary antibodies were used. Arrows indicate the epidermis. At least three separate sections of each mouse skin were stained and analyzed. A total of three mice were used per genotype.

development. This experiment used primarily female mice, because male *Grim-19*$^{-/-}$ mice developed inguinal hernias that impeded their mobility and therefore were excluded from our studies under University of Maryland, Baltimore, Institutional Animal Care and Use Committee regulations. Indeed, it was reported earlier tamoxifen treatment promotes the formation of hernias in wild-type C57BL6 mice (21). As shown in Fig. 3*A*, the *Grim-19*$^{-/-}$ mice had more tumors than *Grim-19*$^{+/+}$mice: At week 10, no tumors were detected in the *Grim-19*$^{+/+}$ mice, but a significantly large number of tumors had appeared in *Grim-19*$^{-/-}$ mice (Fig. 3*B*). A majority of these initial tumors were papillomas, which shredded off after a couple of weeks.

With time, mice in both groups developed tumors (Fig. 3*C*). Significantly, the tumors that developed in the *Grim-19*$^{+/+}$mice were smaller (average size: ~2 mm^3) than those that developed in the *Grim-19*$^{-/-}$ mice (average size: ~6 mm^3). In neither group did 100% of the mice develop tumors (*Discussion*). Most importantly, tumor incidence continued to be significantly higher in the *Grim-19*$^{-/-}$ group than in the *Grim-19*$^{+/+}$ group over the entire period of the experiment ($P < 0.0001$). At the end of the experiment, only 19% of *Grim-19*$^{+/+}$mice developed tumors, in sharp contrast to 66% of *Grim-19*$^{-/-}$ mice. Thus, the loss of Grim-19 significantly increases tumor development.

Skin sections were collected from age-matched tumor-bearing and control mice at the end of week 25 and were stained with H&E. Although a single layer of epidermis and cornified epithelium could be found in the untreated skin area of *Grim-19*$^{+/+}$ and *Grim-19*$^{-/-}$ mice (Fig. 3 *D* and *E*, *Upper*), a multilayered epithelium was found in the tumors of *Grim-19*$^{+/+}$ mice. In the *Grim-19*$^{-/-}$ mice, SCC-like keratoacanthomas and invasive carcinomas were found (Fig. 3 *D* and *E*, *Lower*). Thus, loss of *Grim-19* leads to the formation of invasive SCCs.

Because GRIM-19 inhibits STAT3 activity, and many SCCs require high STAT3 activity for their survival (22–24), we next determined whether active Stat3 (pY^{705}) levels were increased in these tumors. Tumor sections were stained with an antibody that detects the pY^{705}-Stat3 (Fig. 4*A*). As expected no tyrosyl phosphorylation of Stat3 was detected in the untreated skin areas of *Grim-19*$^{+/+}$ and *Grim-19*$^{-/-}$ mice. In tumors derived from *Grim-19*$^{+/+}$ and *Grim-19*$^{-/-}$ mice, several cells were positive for pY^{705}-Stat3. Importantly, there were significantly more pY^{705}-Stat3$^+$ cells per field in tumors derived from *Grim-19*$^{-/-}$ mice (Fig. 4*B*). Quantification of these cells from several tumor sections showed a 300% rise in pY^{705}-Stat3$^+$ tumor cells in *Grim-19*$^{-/-}$ mice as compared with *Grim-19*$^{+/+}$ mice (Fig. 4*B*).

To investigate further the relevance of Stat3 activation to its downstream targets, we stained these sections with an antibody that detects cyclin D1, a protein required for cell-cycle progression (Fig. 4*C*). Untreated skin sections from *Grim-19*$^{+/+}$ and *Grim-19*$^{-/-}$ mice stained weakly with cyclin D1. In the tumors, however, there was a clear increase in cyclin D1 levels as shown by multiple positively stained cells. Interestingly, although most of the cyclin D1 in the *Grim-19*$^{+/+}$ tumors was cytoplasmic, it was nuclear in >95% of cells in the *Grim-19*$^{-/-}$ tumors. The significant increase in the number of cyclin D1-positive cells is consistent with the high Stat3 activity in *Grim-19*$^{-/-}$ tumors (Fig. 4*D*). We found this pattern of expression of both proteins in 70% of the tumors. The rise in the expression of pY^{705}-Stat3 and cyclin D1 also was analyzed and quantified using Western blot analysis of the tumor extracts (Fig. 4*E*). The β-catenin protein was induced in 18% of the tumors; and in 30% of the tumors the expression of enhancer zeste homolog 2 (Ezh2), a histone 3 lysine *N*-methyl transferase involved in chromatin repression and cell proliferation, was induced.

The cell–cell adhesion molecule E-cadherin plays a role in tissue integrity and adhesion (25). We found that it was expressed mostly in epithelial keratinocytes of normal skins (Fig. 4*F*), but E-cadherin expression also was seen in tumors. Notably, the intensity of E-cadherin expression was markedly reduced in tumors derived from *Grim-19*$^{-/-}$ mice as compared with tumors from *Grim-19*$^{+/+}$ mice. This pattern of E-cadherin expression was found in 75% of the tumors analyzed and may indicate a transition from adhesive epithelium to invasive SCC. Last, 18% of *Grim-19*$^{-/-}$ tumors expressed a higher level of β-catenin (Fig. 4*G*), a protein associated with skin tumorigenesis. Most of the β-catenin seen in the wild-type tumors was diffuse in the cytoplasm, but in *Grim-19*$^{-/-}$ tumors β-catenin was found primarily along the membrane. The significance of this finding is unclear.

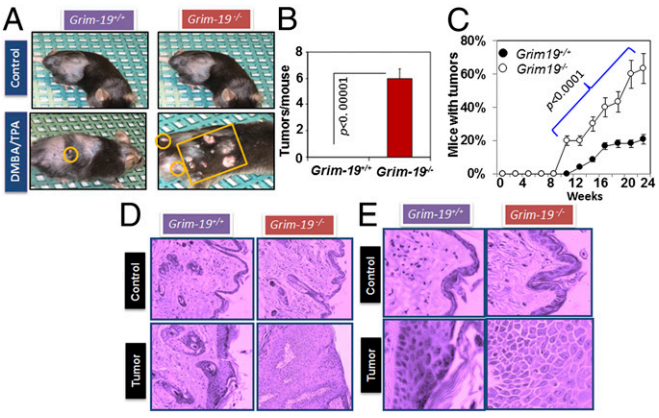

Fig. 3. *Grim-19*$^{-/-}$ mice are hypersensitive to DMBA/TPA-induced carcinogenesis. (*A*) Gross images of mice showing tumor development. Control mice did not receive DMBA/TPA. Tumor locations are indicated by circles or rectangles. (*B*) Quantification of tumors developed 10 wk after DMBA/TPA treatment. (*C*) Time course of tumor development. (*D*) H&E-stained sections of skin and tumor tissues at week 22. (Magnification: 20×.) Note the invasive tumor cells in the tumors of *Grim-19*$^{-/-}$ mice. (*E*) An enlarged view (magnification: 60×) of the tumor and skin sections. Images in *D* and *E* are representative of eight tumors from four different mice per genotype.

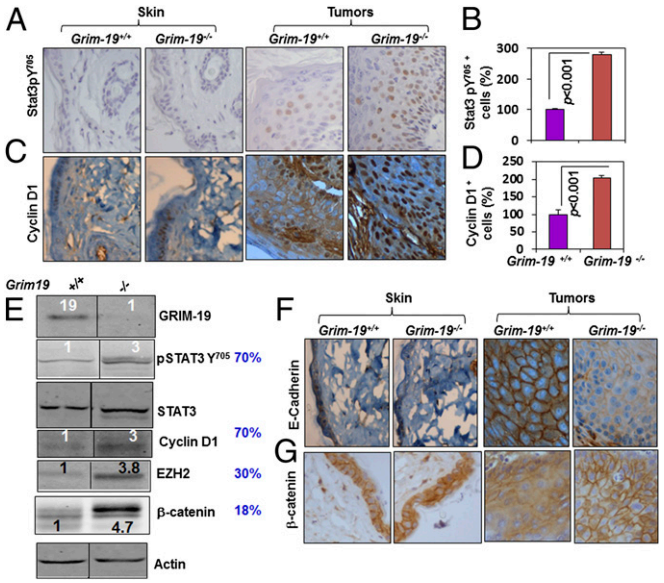

Fig. 4. (*A–D*, *F*, and *G*) Immunohistochemical analyses of tumors with the indicated antibodies. *B* and *D* show quantified data from three sections each from six independent tumors from three different mice. Note the nuclear staining of phospho-STAT3 and cyclin D1 in tumors derived from knockout mice. (*E*) Western blot analyses of tumor extracts with indicated antibodies. Numbers on the blots indicate the relative band intensities (arbitrary units) in each case. Numbers in blue to the right of the blot state the percentage of *Grim-19*$^{-/-}$ tumors expressing the indicated marker.

The Role of Stat3 in *Grim-19*–Dependent Tumorigenesis. To test the biological relevance of Stat3 in driving tumorigenesis, we performed two different experiments. In the first experiment, 10 wk after tumorigenesis was initiated with DMBA/TPA (i.e., at the time when tumors begin to appear), *Grim-19*$^{-/-}$ mice were treated s.c. with DMSO or the STAT3 inhibitor S31-201 (3 mg/kg body weight) twice weekly for an additional 5 wk. Tumor development was observed at the end of experiment. S31-201 caused a significant drop in tumor development (Fig. 5*A*). These results are consistent with a previous report (26) that showed skin-specific deletion of *Stat3* reduced tumor development in response to DMBA/TPA.

In the second experiment we examined whether the loss of *Grim-19* accompanied by a simultaneous up-regulation of constitutively active STAT3 (STAT3C) would enhance carcinogenesis. *Grim-19*$^{f/f}$ mice or *Grim19*$^{+/+}$ mice with *K14-CreER*^{tam} were bred with a mouse expressing STAT3C under the control of the *Rosa26* promoter. In this model, deletion of the *Grim-19*$^{f/f}$ locus and simultaneous activation of STAT3C expression occur after the activation of Cre with 4-HT (Fig. 5*B*). After we confirmed the expected genotypes (Fig. 5*C*), we subjected groups of mice (n = 24) to carcinogenesis with DMBA/TPA. As controls, we used *Grim-19*$^{f/f}$ mice and *Grim19*$^{+/+}$ (*K14-CreER*^{tam} without STAT3C) mice. As expected, loss of *Grim-19* caused a significant increase in carcinogenesis (Fig. 5*D*). In the presence of STAT3C both *Grim-19*$^{-/-}$ and *Grim-19*$^{+/+}$ mice were more susceptible to tumorigenesis than their respective controls. Notably, STAT3C in the *Grim-19*$^{-/-}$ background strongly enhanced tumorigenesis, compared with *Grim-19*$^{+/+}$. In the *Grim-19*$^{-/-}$ background STAT3C promoted the highest level of carcinogenesis compared with the corresponding control without STAT3C. We also noted that tumors appeared significantly earlier in *Grim-19*$^{-/-}$/*STAT3C* mice than in *Grim-19*$^{-/-}$ mice. Neither *Grim-19*$^{-/-}$/*STAT3C* nor *Grim-19*$^{+/+}$/*STAT3C* mice developed any spontaneous tumors at 16 mo.

Increased Expression of Growth-Associated Genes in the Tumors of *Grim-19*$^{-/-}$ Mice. To determine if tumor proliferation is associated with the expression of genes involved in cell growth and survival, we performed a real-time PCR analysis of transcripts coding for cyclins B1 (*Ccnb1*) and D1 (*Ccnd1*), cyclin-dependent kinase 1 (*Cdk1*), dihydrofolate reductase (*Dhfr*), an S-phase enzyme critical for purine nucleotide metabolism, and the cell-survival protein Bcl-X_L (*Bcl2-l1*). The expression of these transcripts was increased significantly (two- to fivefold in individual tumors) in tumors derived from *Grim-19*$^{-/-}$ mice as compared with tumors from *Grim-19*$^{+/+}$ mice (Fig. 6). All these differences were statistically significant (P < 0.01–0.001). Because of the loss of E-cadherin expression, we assumed that these tumors might have acquired an undifferentiated phenotype. Therefore, we measured the expression of the stem cell markers sex-determining region box 2 (*Sox2*), octamer-binding transcription factor 4 (*Oct4*), and *Nanog* in the tumors (27). We could not detect *Oct4,* and *Nanog* in quantitative PCR (qPCR) analyses. *Sox2* levels increased significantly in the *Grim-19*$^{-/-}$ tumors as compared with the *Grim-19*$^{+/+}$ tumors (P < 0.02). Thus, these tumors acquired a stem cell-like feature, albeit not fully.

Loss of a Single *Grim-19* Allele Increases Susceptibility to Tumorigenesis. Based on these observations, we next investigated if the loss of a single *Grim-19* allele also would increase the susceptibility to tumorigenesis. Heterozygous mice carrying wild-type and floxed alleles (*Grim-19*$^{+/f}$) were mated with *K14-Cre* mice to generate mice lacking one *Grim-19* allele (*Grim-19*$^{+/-}$). Fig. 7*A* shows the comparative genotyping of these mice. Fig. 7*B* shows a representative Western blot of skin extracts from these mice. The resultant *Grim-19*$^{+/-}$ mice (n = 17) and control *Grim-19*$^{+/+}$ mice (n = 18) were exposed to DMBA/TPA as described previously. Around week 13, mice in both groups developed papillomas (Fig. 7*C*). At this time more *Grim-19*$^{+/-}$ mice (18%) than *Grim-19*$^{+/+}$ mice (7%) had developed tumors, and thereafter there were significantly more tumor-bearing mice in the *Grim-19*$^{+/-}$ group than in the *Grim-19*$^{+/+}$ group (Fig. 7*D*). At the peak (weeks 19 and 20), 19% of the *Grim-19*$^{+/+}$ mice and 44% of *Grim-19*$^{+/-}$ mice had tumors. This difference in the numbers of tumor-bearing mice was highly significant (P < 0.001), and, on average, there were significantly more tumors per mouse in *Grim-19*$^{+/-}$ mice (P < 0.001) than in *Grim-19*$^{+/+}$ mice (Fig. 7*E*). Histopathologically, these tumors ranged from keratoacanthomas to squamous cell-like carcinomas (Fig. 7*F*).

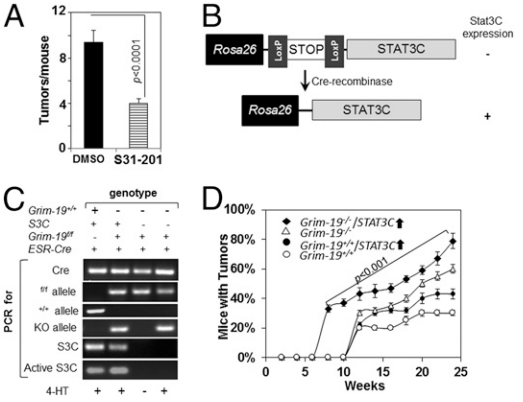

Fig. 5. STAT3 plays a major role in tumorigenesis. (*A*) *Grim-19*$^{-/-}$ mice (n = 10 per group) were treated with DMBA/TPA as described for 10 wk. One group of mice received vehicle (DMSO); the other was treated s.c. with S31-201 (4 mg/kg body weight) twice weekly. Tumor growth was monitored for an additional 5 wk and plotted. (*B*) A schematic diagram showing conditional activation of STAT3C. (*C*) PCR-based genotyping for confirming deletion of *Grim-19* and activation of *STAT3C* in mice. Allele-specific primers were used for PCR with the mouse skin genomic DNA as template. S3C, STAT3C. (*D*) Mice with the indicated genotypes were subjected to carcinogenesis. This experiment shows mean ± SE of three separate experiments and involved 24 mice per genotype.

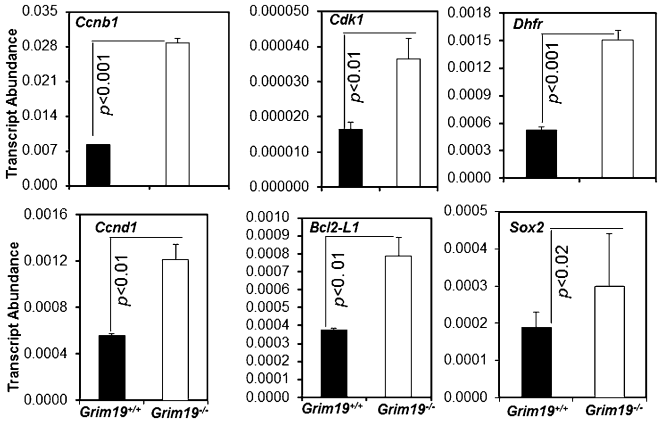

Fig. 6. Real-time PCR analyses of the expression of specific growth-associated gene products in the tumors. Each bar indicates five replicates of RNA from five different tumors. *P* values are indicated.

These tumors also were stained for pY^{705}-Stat3. As expected, there were significantly ($P < 0.01$) higher numbers of pY^{705}-$STAT3^+$ cells in tumors from *Grim-19*$^{+/-}$ mice than in tumors from *Grim-19*$^{+/+}$ mice (Fig. 8 *A* and *B*). This increase in active Stat3 levels in the tumors corresponded to an increase in cyclin D1 levels (Fig. 8 *C* and *D*). About 60% of the tumors had high pY^{705}-STAT3 staining and cyclin D1 expression. As in tumors from *Grim-19*$^{-/-}$ mice, cyclin D1 was exclusively nuclear in the tumors of *Grim-19*$^{+/-}$ mice. No such increase in the levels of active Stat3 and cyclin D1 occurred in the normal skins. Last, the tumorigenic phenotype in *Grim-19*$^{+/-}$ mice also was consistent with a loss of E-cadherin expression (Fig. 8*E*). About 9% of these tumors had high β-catenin expression (Fig. 8*F*). Thus, monoallelic loss of *Grim-19* increases the susceptibility to carcinogenesis in vivo.

Loss of *Grim-19* Causes Dysfunction of the Mitochondrial Electron Transport. Because GRIM-19 also is found as part of the mitochondrial electron transport chain (ETC) complex I, and an earlier report suggested a dysfunction of ETC complexes I and IV in *Grim-19* null cells, we verified these aspects in *Grim-19*$^{+/+}$, *Grim-19*$^{+/-}$, and *Grim-19*$^{-/-}$ tumor cells by measuring glycolysis and mitochondrial respiration in real time using the Seahorse XF24 flux analyzer. By providing exogenous pyruvate and a proton ionophore carbonylcyanide-p-trifluoromethoxyphenylhydrazone (FCCP), we measured basal and maximal O_2 consumption rates (OCR) in cells. As shown in Fig. 9*A*, basal and maximal OCR were reduced significantly in *Grim-19*$^{-/-}$ cells compared with *Grim-19*$^{+/+}$ cells. Importantly, the maximal OCR did not rise despite the provision of exogenous substrates to *Grim-19*$^{-/-}$ cells. Interestingly, there was a significant reduction in basal OCR in *Grim-19*$^{+/-}$ compared with *Grim-19*$^{+/+}$ cells (Fig. 9*B*). However, maximal OCR rose in *Grim-19*$^{+/-}$ cells, unlike *Grim-19*$^{-/-}$ cells (Fig. 9 *A* and *B*). The maximal OCR continued to be lower in *Grim-19*$^{+/-}$ cells than in wild-type cells. Media supernatants from *Grim-19*$^{+/+}$, *Grim-19*$^{+/-}$, and *Grim-19*$^{-/-}$ cells also were used for measuring glucose and lactate levels (Fig. 9 *C* and *D*). Significantly higher glucose consumption and lactate production were observed in *Grim-19*$^{+/-}$ and *Grim-19*$^{-/-}$ cells than in *Grim-19*$^{+/+}$ cells. As expected, such alterations in glucose and lactate were more pronounced in *Grim-19*$^{-/-}$ cells than in *Grim-19*$^{+/-}$ cells.

Last, we have determined the levels of certain important components of various ETC complexes using the Mitoprofile Total OXPHOS monoclonal antibody mixture. The antibodies in this mixture detect NDUFB8, SDHB, UQCRC2, MTCO1, and ATP5α subunits of complexes I–V, respectively, and were chosen because they are antibodies against a subunit that is labile when its complex is not assembled. Loss of *Grim-19* caused a significant decline in the levels of proteins associated with complexes I, II, IV, and V, with complexes I and IV being the most affected (Fig. 9*E*, *Left*). The identity of the band below SDHB is unclear, because it was not present in the positive control lane (rat liver mitochondrial lysate). However, its levels also declined in the absence of *Grim-19*. It is likely a degradation of the product of one of the complexes or a cross-reactive protein in whole-cell lysates. Surprisingly, the levels of UQCRC2, a component of complex III, increased strongly. These differences were not to the result of differential loading of proteins. A similar analysis of the *Grim-19*$^{+/-}$ tumors revealed a strong decline in complexes I and IV, a rise in complex III, and no effect on complexes II and V (Fig. 9*E*, *Right*). A quantification of the bands corresponding to each complex and their relative levels are shown in Fig. 9 *F* and *G*. All differences in the levels of various complexes between *Grim-19*$^{-/-}$ and *Grim-19*$^{+/-}$ cells were statistically significant. Thus, loss of *Grim-19* results in a significant dysfunction of mitochondrial respiration and in aberrantly active glycolysis. Notably, such differences also were observed even under conditions of monoallelic loss.

Loss of *Grim-19* Promotes the Expression of Several Genes Involved in Glycolysis. Because defects in mitochondrial respiration and production of lactic acid (Fig. 9 *C* and *D*) were observed in *Grim-19*–deficient tumors, we next investigated whether changes in the genes coding for glycolytic enzymes also occurred in these tumors. Our RNA-seq data, derived from human head and neck

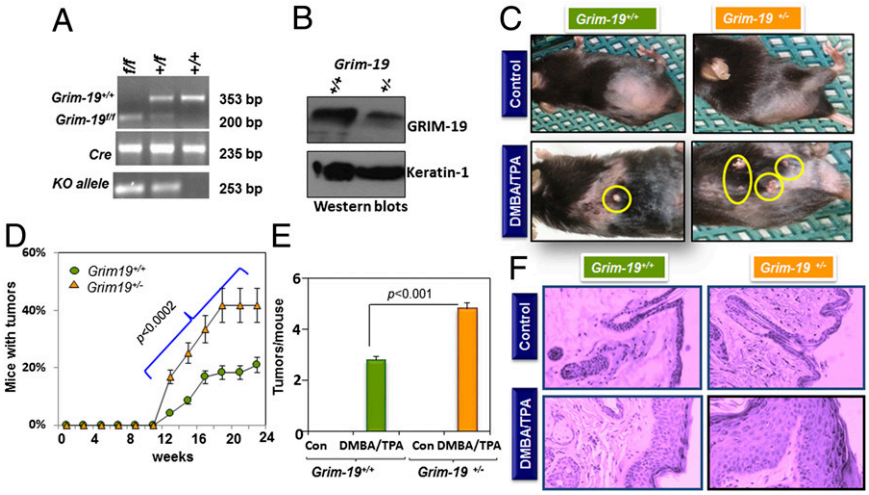

Fig. 7. Monoallelic loss of GRIM-19 is sufficient for promoting tumorigenesis. (*A*) Genotyping of mice. Genomic DNA was subjected to PCR with specific primers after 4-HT treatment.The genotypes of mice and the products are indicated. (*B*) Western blot analyses of the skin extracts after 4-HT treatment. Note a significant loss of GRIM-19 in the heterozygote. (*C*) Gross images of mice showing tumors (yellow circles). (*D*) Kinetics of tumor development after DMBA/TPA treatment. (*E*) Quantified tumor development at 18 wk. (*F*) H&E images of skins and tumors developed. (Magnification: 20×.)

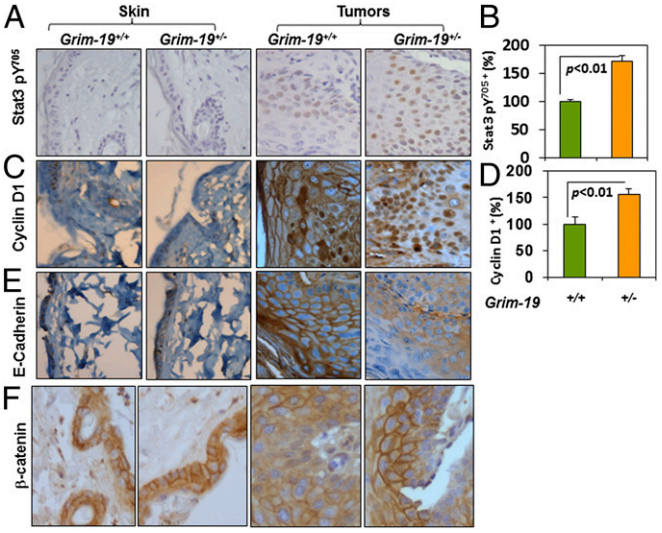

Fig. 8. (*A*, *C*, *E*, and *F*) Immunohistochemical analyses of tumors with the indicated antibodies. Note the nuclear staining of phospho-STAT3 and cyclin D1 in tumors derived from heterozygous mice. (*B* and *D*) Quantified data from two sections from each of four tumors from four different mice. The percentage of cells stained positively was quantified in each case. *P* values also are indicated.

SCCs, showed that genes coding for aldolase A (*ALDOA*), pyruvate kinase, liver and RBC (*PKLR*), glucokinase regulator (*GCKR*), 6-phosphofructo-2-kinase/fructose-2,6-biphosphatase 1 (*PFKFB1*), pyruvate dehydrogenase kinase, isozyme 2 (*PDK2*), and pyruvate dehydrogenase kinase, isozyme 4 (*PDK4*) were induced more than fivefold in *Grim-19*–deficient cells. We have reported recently that the transcript coding for the M2 isoform of pyruvate kinase (*Pkm2*), which is increased in v-Src–transformed rodent fibroblasts, was suppressed by GRIM-19 (28). Therefore, using qPCR, we examined the expression of these genes in tumors that developed in *Grim-19*$^{+/+}$ and *Grim-19*$^{-/-}$ mice. The *Aldoa* (4.2-fold), *Gckr* (3.6-fold), *Pdk2* (4.1-fold), and *Pkm2* (2.4-fold) transcripts were significantly induced in *Grim-19*$^{-/-}$ tumors (Fig. 10 *A*–*D*). Interestingly, expression of *Pdk4* was repressed significantly (Fig. 10*E*) in the absence of *Grim-19*. Because the *Pklr* and *Pfkfb1* primers did not yield any detectable products, we did not present those data here.

Our RNA-seq analysis of *Grim-19*–deleted mouse embryonic fibroblasts showed that several genes are up-regulated in the absence of Grim-19 and others are down-regulated (Table 1). The expression of ATP-binding cassette subfamily B member 5 (*Abcb5*), POU domain, class 2, transcription factor 2 (*Pou2f2*), oligodendrocyte transcription factor 1 (*Olig1*), and carbonic anhydrase 12 (*Car12*) was high in the absence of *Grim-19*. Abcb5 is associated with drug resistance in certain melanomas (29). Pou2f2 (Oct2) promotes resistance to apoptosis via Bcl2 induction (30). Olig1, a basic helix-loop-helix transcription factor, is associated with the development of certain forms of brain tumors (31). *Car12* has been implicated in breast and cervical tumor development (32, 33). This analysis also showed that the expression of certain IFN-stimulated genes (ISGs)—the IFN-induced GTP-binding proteins *Mx1* and *Mx2* and 2′-5′ oligoadenylate synthases 1A (*Oas1a*), 1E (*Oas1e*), and 1H (*Oas1h*)—is down-regulated in the absence of *Grim-19*. These observations are consistent with a previous study that reported repression of several IFN-inducible genes in the presence of STAT3C (34). In light of these findings, we predict that hyperactivated Stat3 resulting from the loss of *Grim-19* mediates such negative effects on ISGs. The relevance to tumor growth of other genes in this analysis is unclear at this stage.

Discussion

It now is clear that the activation of STAT3C, which promotes the growth of cancer cells, requires inactivation/activation of some other factors, apart from phosphorylation of its Y^{705}. Three STAT3 inhibitors, suppressor of cytokine signaling 3 (SOCS3), protein inhibitor of activated STAT3 (PIAS3), and GRIM-19, are known to date. Tumor-suppressive roles have not been established for SOCS3 and PIAS3. Deletion of *Socs3*, which is an inhibitor of Janus kinases, led to defective IL-6 signaling and alterations in IFN-induced responses (35, 36), whereas its overexpression caused resistance to IFN response (37). The biology of the PIAS3 protein is not fully clear. Originally described as a STAT3-specific inhibitor (38), it also blocks the microphthalmia transcription factor (39), acts as a SUMOylation cofactor for nuclear receptors, and binds to the intracellular domain of ErbB4 to enhance its nuclear retention (40). Unlike SOCS3 and PIAS3, which block the acute cytokine-induced responses, GRIM-19 blocks oncogene-induced cellular transformation and acts against chronically active STAT3 (41). Thus, of these three STAT3 inhibitors, GRIM-19 is a likely tumor suppressor.

A potential tumor-suppressor–like activity of GRIM-19 was indicated in our early studies, which found that the same DNA viral oncogenes that inactivate p53 also blocked GRIM-19–induced antigrowth effects. For example, the vIRF1 protein of Kaposi's sarcoma-associated herpesvirus, simian vacuolating virus 40 T antigen, and human papilloma virus-E6 bind to GRIM-19 and block its antitumor effects (42). In high-risk human papilloma virus-positive advanced SCCs of the uterine cervix, loss of GRIM-19 correlated with a loss of tumor-suppressor p53 expression (43). In these tumors, p53 is targeted to ubiquitin/proteasome-dependent degradation by the viral E6 oncoprotein in association with a cellular enzyme, E6AP. GRIM-19 disrupted the formation of E6/E6AP complex to prevent p53 degradation and enforce growth suppression (43). Furthermore, our studies (14) and another independent report (15) showed that GRIM-19 targets transcription factor STAT3 for inhibition via direct

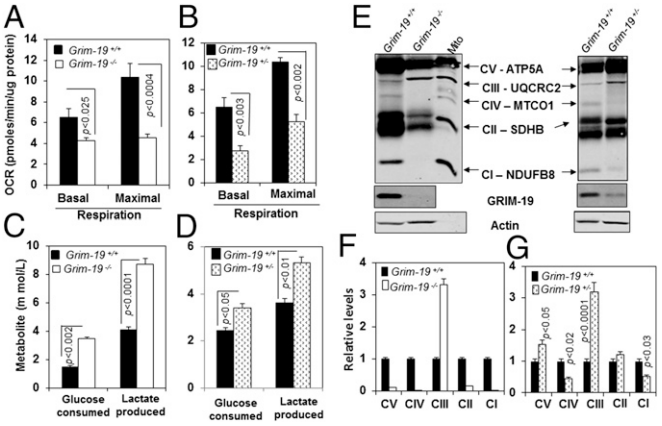

Fig. 9. Impact of Grim-19 deletion on mitochondrial respiration. (*A* and *B*) Tumor cells of the indicated genotypes were analyzed for OCR as described in *SI Appendix*. Basal and maximal respiration indicate the OCR measurements performed in the absence and presence of pyruvate and FCCP. Each bar represents the mean ± SE of 25 samples from five separate experiments. (*C* and *D*) Glucose consumption and lactate production by tumor cells. Spent media were used for measuring metabolite levels after 24 h of growth. Complete medium without cells was used to determine the initial values. Each bar represents the mean ± SE of 15 samples from three experiments. (*E*) OXPHOS blot of tumor lysates. Specific bands and the complexes they belong to are indicated. Mito, rat liver mitochondrial extract (manufacturer-supplied reference standard). Western blots were captured using a LICOR Odyssey infrared imager. (*F* and *G*) Bands corresponding to specific ETC complexes were quantified using the Odyssey imager. Data represent the mean ± SE of three separate tumor samples in each case.

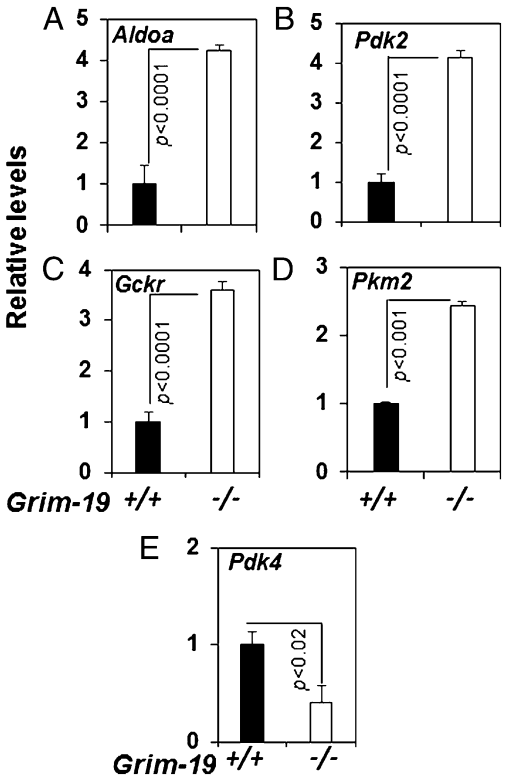

Fig. 10. (*A–E*) Real-time PCR analysis of glycolysis-associated genes. PCR with gene-specific primers was performed as in Fig. 6. *P* values are indicated.

binding. GRIM-19 antagonizes cellular transformation by an experimentally engineered STAT3C (41) and suppresses growth of cell lines expressing high levels of endogenous STAT3C. Direct administration of a plasmid expressing *GRIM-19* into tumors also caused regression (44). GRIM-19 suppressed not only tumor growth but also neoangiogenesis (19). Consistent with its tumor-suppressive characteristics, we and others have documented a loss of GRIM-19 expression in a number of primary human cancers of the kidney, colon, brain, prostate, lung, and cervix (19, 44–51). More recently, we have identified functionally inactivating somatic mutations in *GRIM-19* in primary human oral SCCs (16). *GRIM-19* mutations also have been reported in the Hürthle cell tumors of human thyroid (52). More importantly, all GRIM-19 mutants described to date are ineffective in blocking STAT3 function(s), thus underscoring the importance of GRIM-19 as a tumor suppressor in humans. Previously, the tumor-suppressive activity of GRIM-19 had been established by (*i*) growth suppression in several different tumor cell lines upon its restoration, and (*ii*) its defective expression in primary tumors. Therefore, it is important to know if its loss in the context of a whole animal contributes to tumor development.

Our earlier attempts to knock out the *Grim-19* gene yielded no live pups, consistent with another independent study that reported embryonic lethality at the preimplantation blastocyst stage (53). Cells recovered from the knockout blastocysts showed a suboptimal assembly of ETC complexes I and IV (53). Nonetheless, these studies highlighted the biological importance of GRIM-19 in mitochondrial ATP generation. To circumvent these problems in this study, we generated a mouse that bore a modified *Grim-19* allele that permits its conditional inactivation. Our repeated attempts to generate pan–tissue-deleted mice using a deleter stain, $Meox2^{CreSor}$, which knocks out the target gene later in the embryogenesis (i.e., during somite formation), did not yield any live embryos or pups. As does *Grim-19* deletion, *Stat3* deletion results in embryonic lethality (54), although not at same embryonic stage. Thus, *Grim-19* appears to be important for animal development. One major defect was the defective assembly of mitochondrial ETC complexes I, IV, and V in the absence of *Grim-19* (Fig. 9 *F–H*). Together, these observations suggest that *Grim-19* loss causes low ATP production in the developing embryo, leading to death in utero (53). Indeed, $Grim\text{-}19^{-/-}$ cells consumed less oxygen, used more glucose, and produced higher amounts of lactic acid than did the wild-type cells, suggesting a switch to Warburg respiration. Despite these notable effects on oxidative phosphorylation, deletion of *Grim-19* in the adult skin did not affect skin organization and/or differentiation significantly, because all markers of skin were present equivalently in $Grim\text{-}19^{-/-}$ and control samples (Fig. 2).

Under current experimental conditions, deletion of *Grim-19* alone did not result in tumor development in the skin at 19 mo. It is possible that these mice may develop tumors as they age. However, the knockout mice are extremely susceptible to skin tumorigenesis when exposed to DMBA/TPA. Many of these tumors looked like keratoacanthomas in transition to poorly differentiated SCCs. Complementing our data, an earlier study showed that skin-specific deletion of *Stat3* suppressed skin tumors in response to DMBA/TPA, indicating the critical role of *Stat3* in skin tumorigenesis (26). The level of Stat3 activation was significantly high in the *Grim-19*–deficient tumors, and most of the Stat3 was found in the nuclei. Active Stat3 levels increased in 70% of the $Grim19^{-/-}$ tumors analyzed. However, overexpression of STAT3C alone was insufficient for skin tumorigenesis unless accompanied by treatment with DMBA/TPA (55), suggesting that the inactivation of another tumor suppressor is required. Some recent studies reported the presence of Stat3 in mitochondria of certain cell types and in certain Ras-transformed cells. However, we were unable to find Stat3 in the mitochondria of either $Grim\text{-}19^{-/-}$ or $Grim\text{-}19^{+/+}$ tumors. Consistent with oncogenic alterations in the skin, activated Stat3 levels also were increased, resulting in an increased expression of cyclin D1 (Fig. 4), a transcriptional target of STAT3 (56). We recently reported that acquisition of *GRIM-19* mutations or loss of its expression in primary human tumors unleashes STAT3 activity and up-regulation of cyclin D1 (16). Indeed, pharmacological interference with Stat3 function suppressed tumorigenesis in $Grim\text{-}19^{-/-}$ mice (Fig. 5*A*). Conversely, overexpression of STAT3C significantly promoted tumorigenesis in these mice (Fig. 5*D*). Taken together, these observations indicate important roles for GRIM-19 and STAT3 (57) early in tumorigenesis.

Interestingly, almost all the cyclin D1 is found in the nuclei of the tumors from $Grim19^{-/-}$ mice. In contrast to its canonical role in the cell cycle as a cofactor for certain cyclin-dependent kinases (CDKs), in other models (58, 59), in some cases cyclin D1 acts as a transcriptional coactivator promoting or suppressing gene expression, apparently independently of CDKs (60). Furthermore, certain cyclin–CDK complexes participate in splicing as well as transcription (61) and thus may alter gene expression in cancer cells. In addition to cyclin D1, many growth-promoting genes such as *Bcl2-l1*, *Ccnb1*, *Ccnd1*, *Cdk1*, and *Dhfr* also were highly induced in these tumors. Notably, the first three are known to be regulated by STAT3 (14). Similar to $Grim\text{-}19^{-/-}$ mice, $Stat1^{-/-}$ mice did not develop skin tumors unless exposed to chemical carcinogens (62), indicating that loss of a tumor suppressor alone is insufficient for promoting tumor formation. $Grim19^{-/-}$ tumors appear to be poorly differentiated, as shown by the expression of *Sox*2 (in 30% of tumors), and Ezh2 (in 30% of tumors). Other markers of undifferentiated state such as Nanog and Oct 4 were undetectable in our hands. EZH2 is a histone 3 lysine *N*-methyl transferase belonging to the polycomb group of proteins which causes chromatin repression and is known be up-regulated in a number of human cancers (63). A recent study showed that arsenic-induced carcinogenesis involves the activation of Ezh2 via the JNK/STAT3/Akt pathway (64). Such observations indicate a potential connection between STAT3/GRIM-19 and Ezh2, such that a loss of GRIM-19 may promote Ezh2 up-regulation (Fig. 4*E*). In some nonmelanoma human skin cancers, β-catenin levels are elevated (65) and have been implicated in DMBA/TPA-

Table 1. Changes in gene expression after *Grim-19* deletion

Category	Gene	Description	Fold change in the absence of Grim-19
Intermediary metabolism	*Aldh3a1*	Aldehyde dehydrogenase, dimeric NADP-preferring	> sevenfold decrease
	Sdsl	Serine dehydratase-like	> sixfold decrease
Immunity related	*C1qtnf6*	Complement C1q tumor necrosis factor-related protein 6	> fivefold decrease
	Cx3cl1	Fractalkine	> fivefold decrease
	Cys1	Cystin 1	> fivefold decrease
	IL33	Interleukin-33	> 10-fold decrease
	Mx1	IFN-induced GTP-binding protein Mx1	> sevenfold decrease
	Mx2	IFN-induced GTP-binding protein Mx2	> fivefold decrease
	Nov	CCN protein family - Nephroblastoma overexpressed	> fivefold decrease
	Oas1a	2′-5′ oligoadenylate synthase 1A	> fivefold decrease
	Oas1e	2′-5′ oligoadenylate synthase 1E	> fivefold decrease
	Oas1h	2′-5′ oligoadenylate synthase 1H	> eightfold decrease
	Tnfrsf8	Tumor necrosis factor receptor superfamily member 8	> fourfold decrease
Ion channels	*Abcb5**	ATP-binding cassette subfamily B member 5	> fivefold increase
	Kcnj15	ATP-sensitive inward rectifier potassium channel 15	> sixfold increase
	Kcnma1	Calcium-activated potassium channel subunit alpha-1	> fivefold increase
Transcription	*Pou2f2**	POU domain, class 2, transcription factor 2	> fivefold increase
	Lbx2	Transcription factor LBX2	> fourfold increase
	Sox10	Transcription factor SOX-10	> fourfold increase
	*Olig1**	Oligodendrocyte transcription factor 1	> fourfold increase
Others	*Car12**	Carbonic anhydrase 12	> fivefold increase
	Inpp5j	Phosphatidylinositol 4,5-bisphosphate 5-phosphatase A	> fivefold decrease
	Pcdhga7	Protocadherin gamma-A7	> eightfold decrease
	Tmem200a	Transmembrane protein 200A	> fivefold decrease
	Trhde	TSH-releasing hormone-degrading ectoenzyme	> sevenfold decrease
	Umodl1	Uromodulin-like 1	> sevenfold decrease
	Vcam1	Vascular cell adhesion protein 1	> sevenfold decrease

Decrease = loss of transcript levels.
*Cancer-associated expression.

induced skin tumor development (66). In 18% of tumors developed in *Grim19*$^{-/-}$ mice we observed a rise in β-catenin protein (Fig. 4*G*). Thus, β-catenin expression appears to be a minor pathway activated in *Grim19*$^{-/-}$ tumors.

Recent studies with skin-specific *Stat*3 knockout and transgenes have shown that Stat3 plays a key role in DMBA/TPA-induced carcinogenesis, resulting in the development of SCCs (26, 55). Indeed, a positive correlation between phospho-STAT3 and the invasive potential of nonmelanoma cutaneous SCCs has been found in human studies (22). Similarly, in head and neck SCCs STAT3 is critical for initiation and progression of disease (57). As mentioned previously, GRIM-19 mutants from human oral SCCs were significantly weak at inhibiting STAT3 activity (16). Last, E-cadherin expression was reduced significantly in the tumors that developed in *Grim19*$^{-/-}$ mice as compared with those in wild-type mice. Such reduction in E-cadherin is consistent with the invasive phenotype of these SCCs (25). Together these data suggest that deregulation of STAT3 is a clear first step in carcinogenesis, thus placing Grim-19 and Stat3 in the early stages of carcinogenesis. In this regard, *Grim-19*$^{-/-}$ mice behaved like *Stat1*$^{-/-}$ mice, which also are hypersensitive to chemical carcinogenesis. However, unlike *STAT1*, loss of expression and mutations in *GRIM-19* occur in human tumors. One surprising observation that emerged from our studies is that even a monoallelic loss of *Grim-19* is sufficient for tumor development. Mice bearing single alleles of many tumor suppressors such as *Beclin1* (67, 68), *Mapsin* (69), *Pten* (70), *Atr* (71), *Anx7* (72), and *Blm* (73) are similarly prone to tumor development.

Tumor arising in DMBA/TPA-treated skins generally carry mutations in the Harvey rat sarcoma (*Hras*) gene, particularly in one of the amino acids at codons 12 or 61, which code for Gly and Gln, respectively (74). Sequencing of the *Hras* gene from six different tumors each from wild-type and *Grim-19*$^{-/-}$ mice revealed acquisition of heterozygosity in *Hras* gene. Irrespective of the *Grim-19* genotype, all tumors except one bore mutations at codon 61, where Gln was replaced by either Leu or His. Only one tumor had a Gly-to-Val substitution at codon 12. Thus, loss of *Grim-19* does not seem to alter the spectrum of *Hras* mutations. Importantly, *Hras* mutation alone is insufficient to promote skin tumorigenesis without another genetic change. Last, under the conditions used in our study, only 68% of *Grim-19*$^{-/-}$ mice developed tumors. This result probably does not reflect a lack of 100% penetrance of the gene effect, because laboratory strains of mice respond differently to DMBA/TPA. The DMBA/TPA sensitivity of different strains of mice is in the following order: Sencar > NMR1 > CD1 > C57BL6, with Sencar being the most sensitive (74). Despite the weaker response of the C57BL6 stain to DMBA/TPA, we were able to observe distinct differences between the wild-type and *Grim-19*$^{-/-}$ mice.

The mitochondrial ATP production occurs via four well-defined ETC complexes plus the ATP synthase. We found that loss of *Grim-19* dramatically affected mitochondrial respiration and glucose metabolism (Figs. 9 and 10). After *Grim-19* deletion, the assembly of nearly all ETC complexes was defective, with a rise in complex III (Fig. 9 *E–G*). Earlier, it was reported that in certain primary human renal cell carcinomas (RCCs), loss of ETC activity resulting from a decline in the levels of complexes II–V was associated with tumor aggressiveness (75), although the reason for the association was unknown. Importantly, we have reported that a loss of GRIM-19 (present in complex I) in RCCs promotes tumor growth (76). The mammalian ETC complex I consists of ∼46 subunits, 14 of which form the catalytic core (77). Seven of the core subunits are derived from the mitochondrial and nuclear genomes. The rest, the so-called "accessory subunits," are derived primarily from the nuclear genome and are suggested to guard the integrity of this complex. For example, the NDUFA4 subunit stimulates NADH-ubiquinone reductase activity (77). Consistent with these observations, we observed a significant loss of all complexes, with a more dramatic effect on complexes I and IV. Thus, GRIM-19 appears to guard the in-

tegrity of ETC complexes, because its absence affected not only complex I but also the others. Such loss may be secondary to the inability to form complex I. Taken together, these findings suggest that the loss GRIM-19 may be an early step in ETC dysfunction. Biologically, inhibition of ETC resulting from mutations in one of its subunits or in their assembly or from RNAi-mediated suppression causes resistance to apoptosis (see ref. 78 for a review). For example, mutations in the SDH-B/C/D, the components of complex II, are found commonly in certain pheochromocytomas, paragangliomas, and RCCs (79, 80) and are associated with resistance to apoptosis and tumorigenesis (78). In agreement with these observations, we have demonstrated in previous studies (13, 16, 76) that loss of GRIM-19 expression or mutations involving GRIM-19 cause resistance to apoptosis and promotion of cell growth. Although some recent studies have reported Stat3 as a necessary protein for complex II function in certain Ras-transformed cells (81), we have not observed mitochondrial Stat3 in either wild-type or *Grim-19*$^{-/-}$ tumors. Importantly, it appears that GRIM-19 loss favors a dependence on glycolysis and an avoidance of apoptosis, two major landmarks of an evolved cancer cell.

Our analysis of genes coding for glycolysis showed that Aldoa, Gckr, Pkm2, and Pdk2 are induced strongly in the absence of Grim-19. Aldolase (A, B, and C isoforms) catalyzes the reversible cleavage of fructose-1, 6-(bis) phosphate and fructose 1-phosphate to dihydroxyacetone phosphate and either glyceraldehyde-3-phosphate or glyceraldehyde, respectively. Several studies have shown that high ALDOA levels drive cell proliferation (82, 83). Notably, a nonglycolytic nuclear role for ALDOA in transcription (83) and a role in cytokinesis, independent of its catalytic function (82) have been suggested, although the pertinent target factors have not been identified. The PKM gene codes two alternately spliced gene products, M1 and M2. The latter is found primarily during embryonic development but reappears in a number of human cancers and aids in lactate production. Interestingly, recent studies show that this protein modulates histone phosphorylation (84) and acts as a coactivator for several transcription factors such as HIF1, HIF2, β-catenin (85), Oct4, and STAT3 (86). Dimeric PKM2, a form found predominantly in the nuclei, unlike the tetrameric form found in the cytoplasm, directly phosphorylates STAT3-Y^{705}, independent of JAKs and Src, to promote transcription of cellular genes and tumor formation (86). Based on these observations, we suggest that Pkm2 may serve as a nuclear transcriptional modulator of Stat3 in the absence of *Grim-19*. Indeed, nuclear PKM2 has been suggested to be a poor prognosticator for certain head and neck SCCs (87). Four isozymes of PDK are described to date. Among these, expression of PDK1, which promotes lactate production and hypoxia, is associated with a poor prognosis for certain head and neck SCCs (88). Chronic exposure of keratinocytes to cigarette smoke induces PDK2 expression, hypoxia, and increased glycolysis (89). The tumor suppressor p53 negatively regulates PDK2, indicating its potent tumor-promoting function (90). These observations are consistent with the elevated expression of *Pdk2* in the absence of *Grim-19*. This elevated expression appears to be a selective effect on *Pdk2*, given the down-regulation of *Pdk4* in the absence of *Grim-19* (Fig. 10*E*). It has been reported that PDK4 is down-regulated in presence of STAT3 (34). That Stat3 activity goes up in the absence of *Grim-19* is consistent with the repression of *Pdk4.* The role of GCKR in cancer is unknown, except that a single polymorphism associated with diabetes is associated with an increased risk for the development of pancreatic cancer (91).

Loss of Grim-19 appears to alter tumor microenvironment. Enhanced glycolysis in the absence of *Grim-19* led to the production of lactic acid (Fig. 9). Lactic acid secreted by tumors is known to promote tumor growth by inducing inflammation, angiogenesis, tumor cell motility, and immune escape (92). In contrast, tumor-derived lactic acid has been shown to suppress T cells (93). Activated T cells themselves generate energy through glycolysis. When tumor cells release large quantities of lactate into their microenvironment, immune cells cannot rid themselves of their own lactate, because cellular lactate secretion is dependent on the ratio of intra- to extracellular concentration (92). As a result, lymphocytes may be inactivated by lactate. In summary, our studies provide compelling evidence that *Grim-19* has a major role in tumor suppression by acting as an essential regulator of antioncogenic transcription and metabolism.

Materials and Methods

All experimental procedures were approved by the University of Maryland, Baltimore, Institutional Animal Care and Use Committee. All data were subjected to Student's paired *t* test. A P value < 0.05 was considered significant in all experiments. Detailed materials and methods are presented in the *SI Appendix*.

ACKNOWLEDGMENTS. We thank Klaus Rajewsky for providing Rosa26-LoxP-STOP-LoxP-STAT3C mice. These studies were supported by National Institutes of Health Grant CA105005 (to D.V.K.).

1. Hanahan D, Weinberg RA (2011) Hallmarks of cancer: The next generation. *Cell* 144 (5):646–674.
2. Kalvakolanu DV (2004) The GRIMs: A new interface between cell death regulation and interferon/retinoid induced growth suppression. *Cytokine Growth Factor Rev* 15(2-3):169–194.
3. Vesely MD, Kershaw MH, Schreiber RD, Smyth MJ (2011) Natural innate and adaptive immunity to cancer. *Annu Rev Immunol* 29:235–271.
4. Critchley-Thorne RJ, et al. (2009) Impaired interferon signaling is a common immune defect in human cancer. *Proc Natl Acad Sci USA* 106(22):9010–9015.
5. Burnette BC, et al. (2011) The efficacy of radiotherapy relies upon induction of type i interferon-dependent innate and adaptive immunity. *Cancer Res* 71(7):2488–2496.
6. Weichselbaum RR, et al. (2008) An interferon-related gene signature for DNA damage resistance is a predictive marker for chemotherapy and radiation for breast cancer. *Proc Natl Acad Sci USA* 105(47):18490–18495.
7. Chan SR, et al. (2012) STAT1-deficient mice spontaneously develop estrogen receptor α-positive luminal mammary carcinomas. *Breast Cancer Res* 14(1):R16.
8. Taniguchi T, Lamphier MS, Tanaka N (1997) IRF-1: The transcription factor linking the interferon response and oncogenesis. *Biochim Biophys Acta* 1333(1):M9–M17.
9. Bidwell BN, et al. (2012) Silencing of Irf7 pathways in breast cancer cells promotes bone metastasis through immune escape. *Nat Med* 18(8):1224–1231.
10. Holtschke T, et al. (1996) Immunodeficiency and chronic myelogenous leukemia-like syndrome in mice with a targeted mutation of the ICSBP gene. *Cell* 87(2):307–317.
11. Willman CL, et al. (1993) Deletion of IRF-1, mapping to chromosome 5q31.1, in human leukemia and preleukemic myelodysplasia. *Science* 259(5097):968–971.
12. Schmidt M, et al. (1998) Lack of interferon consensus sequence binding protein (ICSBP) transcripts in human myeloid leukemias. *Blood* 91(1):22–29.
13. Angell JE, Lindner DJ, Shapiro PS, Hofmann ER, Kalvakolanu DV (2000) Identification of GRIM-19, a novel cell death-regulatory gene induced by the interferon-beta and retinoic acid combination, using a genetic approach. *J Biol Chem* 275(43): 33416–33426.
14. Zhang J, et al. (2003) The cell death regulator GRIM-19 is an inhibitor of signal transducer and activator of transcription 3. *Proc Natl Acad Sci USA* 100(16): 9342–9347.
15. Lufei C, et al. (2003) GRIM-19, a death-regulatory gene product, suppresses Stat3 activity via functional interaction. *EMBO J* 22(6):1325–1335.
16. Nallar SC, et al. (2013) Tumor-derived mutations in the gene associated with retinoid interferon-induced mortality (GRIM-19) disrupt its anti-signal transducer and activator of transcription 3 (STAT3) activity and promote oncogenesis. *J Biol Chem* 288(11):7930–7941.
17. Lippman SM, et al. (1992) 13-cis-retinoic acid plus interferon alpha-2a: Highly active systemic therapy for squamous cell carcinoma of the cervix. *J Natl Cancer Inst* 84(4): 241–245.
18. Lippman SM, et al. (1992) 13-cis-retinoic acid and interferon alpha-2a: Effective combination therapy for advanced squamous cell carcinoma of the skin. *J Natl Cancer Inst* 84(4):235–241.
19. Zhou Y, et al. (2009) Down-regulation of GRIM-19 expression is associated with hyperactivation of STAT3-induced gene expression and tumor growth in human cervical cancers. *J Interferon Cytokine Res* 29(10):695–703.
20. Hecht SS (2002) Tobacco smoke carcinogens and breast cancer. *Environ Mol Mutagen* 39(2-3):119–126.
21. Iguchi T, Irisawa S, Uchima FD, Takasugi N (1988) Permanent chondrification in the pelvis and occurrence of hernias in mice treated neonatally with tamoxifen. *Reprod Toxicol* 2(2):127–134.
22. Suiqing C, Min Z, Lirong C (2005) Overexpression of phosphorylated-STAT3 correlated with the invasion and metastasis of cutaneous squamous cell carcinoma. *J Dermatol* 32(5):354–360.

23. Chan KS, et al. (2004) Epidermal growth factor receptor-mediated activation of Stat3 during multistage skin carcinogenesis. *Cancer Res* 64(7):2382–2389.
24. Pedranzini L, Leitch A, Bromberg J (2004) Stat3 is required for the development of skin cancer. *J Clin Invest* 114(5):619–622.
25. Jeanes A, Gottardi CJ, Yap AS (2008) Cadherins and cancer: How does cadherin dysfunction promote tumor progression? *Oncogene* 27(55):6920–6929.
26. Chan KS, et al. (2004) Disruption of Stat3 reveals a critical role in both the initiation and the promotion stages of epithelial carcinogenesis. *J Clin Invest* 114(5):720–728.
27. Takahashi K, et al. (2007) Induction of pluripotent stem cells from adult human fibroblasts by defined factors. *Cell* 131(5):861–872.
28. Kalakonda S, et al. (2013) GRIM-19 mutations fail to inhibit v-Src-induced oncogenesis. *Oncogene*, 10.1038/onc.2013.271.
29. Fukunaga-Kalabis M, Herlyn M (2012) Beyond ABC: Another mechanism of drug resistance in melanoma side population. *J Invest Dermatol* 132(10):2317–2319.
30. Heckman CA, Duan H, Garcia PB, Boxer LM (2006) Oct transcription factors mediate t(14;18) lymphoma cell survival by directly regulating bcl-2 expression. *Oncogene* 25(6):888–898.
31. Aguirre-Cruz L, et al. (2004) Analysis of the bHLH transcription factors Olig1 and Olig2 in brain tumors. *J Neurooncol* 67(3):265–271.
32. Barnett DH, et al. (2008) Estrogen receptor regulation of carbonic anhydrase XII through a distal enhancer in breast cancer. *Cancer Res* 68(9):3505–3515.
33. Yoo CW, et al. (2010) Carbonic anhydrase XII expression is associated with histologic grade of cervical cancer and superior radiotherapy outcome. *Radiat Oncol* 5:101.
34. Dauer DJ, et al. (2005) Stat3 regulates genes common to both wound healing and cancer. *Oncogene* 24(21):3397–3408.
35. Croker BA, et al. (2003) SOCS3 negatively regulates IL-6 signaling in vivo. *Nat Immunol* 4(6):540–545.
36. Lang R, et al. (2003) SOCS3 regulates the plasticity of gp130 signaling. *Nat Immunol* 4(6):546–550.
37. Sakai I, Takeuchi K, Yamauchi H, Narumi H, Fujita S (2002) Constitutive expression of SOCS3 confers resistance to IFN-alpha in chronic myelogenous leukemia cells. *Blood* 100(8):2926–2931.
38. Chung CD, et al. (1997) Specific inhibition of Stat3 signal transduction by PIAS3. *Science* 278(5344):1803–1805.
39. Levy C, Nechushtan H, Razin E (2002) A new role for the STAT3 inhibitor, PIAS3: A repressor of microphthalmia transcription factor. *J Biol Chem* 277(3):1962–1966.
40. Sundvall M, et al. (2012) Protein inhibitor of activated STAT3 (PIAS3) protein promotes SUMOylation and nuclear sequestration of the intracellular domain of ErbB4 protein. *J Biol Chem* 287(27):23216–23226.
41. Kalakonda S, et al. (2007) Tumor-suppressive activity of the cell death activator GRIM-19 on a constitutively active signal transducer and activator of transcription 3. *Cancer Res* 67(13):6212–6220.
42. Seo T, et al. (2002) Viral interferon regulatory factor 1 of Kaposi's sarcoma-associated herpesvirus interacts with a cell death regulator, GRIM19, and inhibits interferon/retinoic acid-induced cell death. *J Virol* 76(17):8797–8807.
43. Zhou Y, et al. (2011) GRIM-19 disrupts E6/E6AP complex to rescue p53 and induce apoptosis in cervical cancers. *PLoS ONE* 6(7):e22065.
44. Zhang L, et al. (2008) Effects of plasmid-based Stat3-specific short hairpin RNA and GRIM-19 on PC-3M tumor cell growth. *Clin Cancer Res* 14(2):559–568.
45. Gong LB, et al. (2007) [Correlations of GRIM-19 and its target gene product STAT3 to malignancy of human colorectal carcinoma]. *Ai Zheng* 26(7):683–687.
46. Zhou AM, et al. (2009) [Expression and clinical significance of GRIM-19 in non-small cell lung cancer]. *Ai Zheng* 28(4):431–435.
47. Okamoto T, et al. (2010) Overexpression of GRIM-19 in cancer cells suppresses STAT3-mediated signal transduction and cancer growth. *Mol Cancer Ther* 9(8):2333–2343.
48. Hao H, et al. (2012) Depletion of GRIM-19 accelerates hepatocellular carcinoma invasion via inducing EMT and loss of contact inhibition. *J Cell Physiol* 227(3):1212–1219.
49. Zhang Y, et al. (2011) Downregulation of GRIM-19 promotes growth and migration of human glioma cells. *Cancer Sci* 102(11):1991–1999.
50. Fan XY, Jiang ZF, Cai L, Liu RY (2012) Expression and clinical significance of GRIM-19 in lung cancer. *Med Oncol* 29(5):3183–3189.
51. Li F, et al. (2012) Downregulation of GRIM-19 is associated with hyperactivation of p-STAT3 in hepatocellular carcinoma. *Med Oncol* 29(5):3046–3054.
52. Máximo V, et al. (2005) Somatic and germline mutation in GRIM-19, a dual function gene involved in mitochondrial metabolism and cell death, is linked to mitochondrion-rich (Hurthle cell) tumours of the thyroid. *Br J Cancer* 92(10):1892–1898.
53. Huang G, et al. (2004) GRIM-19, a cell death regulatory protein, is essential for assembly and function of mitochondrial complex I. *Mol Cell Biol* 24(19):8447–8456.
54. Akira S (2000) Roles of STAT3 defined by tissue-specific gene targeting. *Oncogene* 19(21):2607–2611.
55. Chan KS, et al. (2008) Forced expression of a constitutively active form of Stat3 in mouse epidermis enhances malignant progression of skin tumors induced by two-stage carcinogenesis. *Oncogene* 27(8):1087–1094.
56. Leslie K, et al. (2006) Cyclin D1 is transcriptionally regulated by and required for transformation by activated signal transducer and activator of transcription 3. *Cancer Res* 66(5):2544–2552.
57. Masuda M, et al. (2010) Stat3 orchestrates tumor development and progression: The Achilles' heel of head and neck cancers? *Curr Cancer Drug Targets* 10(1):117–126.
58. Jian Y, et al. (2005) Cyclin D3 interacts with vitamin D receptor and regulates its transcription activity. *Biochem Biophys Res Commun* 335(3):739–748.
59. Ratineau C, Petry MW, Mutoh H, Leiter AB (2002) Cyclin D1 represses the basic helix-loop-helix transcription factor, BETA2/NeuroD. *J Biol Chem* 277(11):8847–8853.
60. Zwijsen RM, et al. (1997) CDK-independent activation of estrogen receptor by cyclin D1. *Cell* 88(3):405–415.
61. Loyer P, Trembley JH, Katona R, Kidd VJ, Lahti JM (2005) Role of CDK/cyclin complexes in transcription and RNA splicing. *Cell Signal* 17(9):1033–1051.
62. Kaplan DH, et al. (1998) Demonstration of an interferon gamma-dependent tumor surveillance system in immunocompetent mice. *Proc Natl Acad Sci USA* 95(13):7556–7561.
63. Bachmann IM, et al. (2006) EZH2 expression is associated with high proliferation rate and aggressive tumor subgroups in cutaneous melanoma and cancers of the endometrium, prostate, and breast. *J Clin Oncol* 24(2):268–273.
64. Chen B, et al. (2013) JNK and STAT3 signaling pathways converge on Akt-mediated phosphorylation of EZH2 in bronchial epithelial cells induced by arsenic. *Cell Cycle* 12(1):112–121.
65. Tataroglu C, Karabacak T, Apa DD (2007) Beta-catenin and CD44 expression in keratoacanthoma and squamous cell carcinoma of the skin. *Tumori* 93(3):284–289.
66. Bhatia N, Spiegelman VS (2005) Activation of Wnt/beta-catenin/Tcf signaling in mouse skin carcinogenesis. *Mol Carcinog* 42(4):213–221.
67. Yue Z, Jin S, Yang C, Levine AJ, Heintz N (2003) Beclin 1, an autophagy gene essential for early embryonic development, is a haploinsufficient tumor suppressor. *Proc Natl Acad Sci USA* 100(25):15077–15082.
68. Qu X, et al. (2003) Promotion of tumorigenesis by heterozygous disruption of the beclin 1 autophagy gene. *J Clin Invest* 112(12):1809–1820.
69. Shao LJ, Shi HY, Ayala G, Rowley D, Zhang M (2008) Haploinsufficiency of the maspin tumor suppressor gene leads to hyperplastic lesions in prostate. *Cancer Res* 68(13):5143–5151.
70. Kwabi-Addo B, et al. (2001) Haploinsufficiency of the Pten tumor suppressor gene promotes prostate cancer progression. *Proc Natl Acad Sci USA* 98(20):11563–11568.
71. Fang Y, et al. (2004) ATR functions as a gene dosage-dependent tumor suppressor on a mismatch repair-deficient background. *EMBO J* 23(15):3164–3174.
72. Srivastava M, et al. (2003) Haploinsufficiency of Anx7 tumor suppressor gene and consequent genomic instability promotes tumorigenesis in the Anx7(+/-) mouse. *Proc Natl Acad Sci USA* 100(24):14287–14292.
73. Goss KH, et al. (2002) Enhanced tumor formation in mice heterozygous for Blm mutation. *Science* 297(5589):2051–2053.
74. Schwarz M, Munzel PA, Braeuning A (2013) Non-melanoma skin cancer in mouse and man. *Arch Toxicol* 87(5):783–798.
75. Simonnet H, et al. (2002) Low mitochondrial respiratory chain content correlates with tumor aggressiveness in renal cell carcinoma. *Carcinogenesis* 23(5):759–768.
76. Alchanati I, et al. (2006) A proteomic analysis reveals the loss of expression of the cell death regulatory gene GRIM-19 in human renal cell carcinomas. *Oncogene* 25(54):7138–7147.
77. Pagniez-Mammeri H, et al. (2012) Mitochondrial complex I deficiency of nuclear origin I. Structural genes. *Mol Genet Metab* 105(2):163–172.
78. Lemarie A, Grimm S (2011) Mitochondrial respiratory chain complexes: Apoptosis sensors mutated in cancer? *Oncogene* 30(38):3985–4003.
79. Baysal BE, et al. (2000) Mutations in SDHD, a mitochondrial complex II gene, in hereditary paraganglioma. *Science* 287(5454):848–851.
80. Ricketts C, et al. (2008) Germline SDHB mutations and familial renal cell carcinoma. *J Natl Cancer Inst* 100(17):1260–1262.
81. Gough DJ, et al. (2009) Mitochondrial STAT3 supports Ras-dependent oncogenic transformation. *Science* 324(5935):1713–1716.
82. Ritterson Lew C, Tolan DR (2012) Targeting of several glycolytic enzymes using RNA interference reveals aldolase affects cancer cell proliferation through a non-glycolytic mechanism. *J Biol Chem* 287(51):42554–42563.
83. Mamczur P, Gamian A, Kolodziej J, Dziegiel P, Rakus D (2013) Nuclear localization of aldolase A correlates with cell proliferation. *Biochim Biophys Acta* 1833(12):2812–2822.
84. Yang W, et al. (2012) PKM2 phosphorylates histone H3 and promotes gene transcription and tumorigenesis. *Cell* 150(4):685–696.
85. Yang W, et al. (2011) Nuclear PKM2 regulates β-catenin transactivation upon EGFR activation. *Nature* 480(7375):118–122.
86. Gao X, Wang H, Yang JJ, Liu X, Liu ZR (2012) Pyruvate kinase M2 regulates gene transcription by acting as a protein kinase. *Mol Cell* 45(5):598–609.
87. Zhang X, et al. (2013) Nuclear PKM2 expression predicts poor prognosis in patients with esophageal squamous cell carcinoma. *Pathol Res Pract* 209(8):510–515.
88. Wigfield SM, et al. (2008) PDK-1 regulates lactate production in hypoxia and is associated with poor prognosis in head and neck squamous cancer. *Br J Cancer* 98(12):1975–1984.
89. Sun W, Chang SS, Fu Y, Liu Y, Califano JA (2011) Chronic CSE treatment induces the growth of normal oral keratinocytes via PDK2 upregulation, increased glycolysis and HIF1α stabilization. *PLoS ONE* 6(1):e16207.
90. Contractor T, Harris CR (2012) p53 negatively regulates transcription of the pyruvate dehydrogenase kinase Pdk2. *Cancer Res* 72(2):560–567.
91. Prizment AE, Gross M, Rasmussen-Torvik L, Peacock JM, Anderson KE (2012) Genes related to diabetes may be associated with pancreatic cancer in a population-based case-control study in Minnesota. *Pancreas* 41(1):50–53.
92. Gottfried E, Kreutz M, Mackensen A (2012) Tumor metabolism as modulator of immune response and tumor progression. *Semin Cancer Biol* 22(4):335–341.
93. Fischer K, et al. (2007) Inhibitory effect of tumor cell-derived lactic acid on human T cells. *Blood* 109(9):3812–3819.